Progress In Electromagnetics Research, Vol. 115, 381–397, 2011

DUAL-BAND TERAHERTZ METAMATERIAL ABSORBER WITH POLARIZATION INSENSITIVITY AND WIDE INCIDENT ANGLE

X.-J. He, Y. Wang, J.-M. Wang, and T.-L. Gui

School of Applied Sciences
Harbin University of Science and Technology
Harbin 150080, China

Q. Wu

School of Electronic Information Engineering
Harbin Institute of Technology
Harbin 150001, China

Abstract—This paper presents the design, simulation and measurement of a dual-band terahertz metamaterial absorber with polarization-insensitivity and wide incident angle. The unit cell of the metamaterial consists of top resonator structures and low metallic ground plane, separated by an isolation material spacer to realize both electric and magnetic resonances. The physical mechanism of dual-band absorption and the sensitivity to the polarization direction and incident direction of the EM wave are theoretically investigated by simulating the x-component and normal component electric field distribution, current distribution on ERRs and metallic ground plane, and distribution of power flow and loss at the resonance frequencies as well as different modes EM waves, based the FDTD calculated method, respectively. The results show that the absorber is not only correctly coupling to the incident electric field and magnetic field, but also can trap the input power into specific positions of the devices and absorb it, besides insensitivity to the polarized angle and incident angle. Moreover, the experiment demonstrates that the absorber achieves two strong absorptions of 82.8% and 86.8% near 1.724 and 3.557 THz.

Received 23 February 2011, Accepted 2 April 2011, Scheduled 8 April 2011
Corresponding author: Xun-Jun He (hexunjun@yahoo.com.cn).

1. INTRODUCTION

The metamaterials are usually defined as a class of artificial media, which compose of the subwavelength structures arranged in periodical arrays and exhibit some extraordinary electromagnetic (EM) properties not available in nature, including single or dual negative properties, backward propagation, and reverse Doppler effects and so on [1–3]. As a new type of artificial materials, it can be applied to many disciplines, which rely on the negative properties described above, such as surperlenses [4, 5], antennas [6, 7], filters [8–10], as well as other devices [11, 12]. However, there are obstacles in the realization of these schemes especially at high frequencies such as terahertz and optical bands, due to exhibiting greater conductive loss of metal [13].

On contrary, the use of metamaterial as microwave absorber has recently attracted considerable attentions by adjusting the refraction index and impedance of the matematerial to maximize the metamaterial losses, and finally realizes EM wave strong absorption [14–17]. This type of absorber has exhibited attractive features which are not available from conventional absorbers. One is in the flexible manipulation of the electromagnetic properties, which realizes more flexible design option. Another is that the matematerial makes the absorber substrate thicknesses significantly smaller, which solves the traditional limitation of the physical size remarkably due to the diffraction. Moreover, the progress of the metamaterial absorber design has been extended from microwave to terahertz frequencies.

So far, various types of terahertz metamaterial absorbers have been reported for applications, like spectroscopy, detector, medical imaging and so on. For example, Tao and his group successfully extended the absorption frequency to 1.3 THz [18], and fabricated a terahertz metamaterial absorber with a wide incident angles for both TE and TM modes [19]. Landy realized a polarization insensitive terahertz metamaterial absorber [20]. Gu et al. presented a wide-band, polarization-insensitive, wide-angle terahertz metamaterial absorber [21]. These metamaterial absorbers show excellent absorption at terahertz frequencies, but they have only one single-band absorption response, which limits the potential application to spectroscopic detection and phase imaging of prohibited drugs and explosive materials that require distinct absorption or fingerprints at multi-frequency [22, 23]. To the best of our knowledge, currently there are only few articles reporting about multiband terahertz metamaterial absorber [24, 25]. Therefore, design and fabrication of multiband terahertz absorber are considerably useful and attractive in the development of terahertz spectroscopic imagers/detectors [26, 27].

In this paper, a dual-band metamaterial absorber with polarization insensitivity and wide incident angle is presented based on perfect impedance-matched to the free space at terahertz frequency range. The simulation based on finite-difference time-domain (FDTD) calculated method is carried out to explore the physical mechanism by the distributions of electronic field, current, power flow and loss, and effect of polarized and incident directions of incident transverse electric (TE) or transverse magnetic (TM) wave on the absorption characteristics of the absorber. The experiment is also carried out to further verify the dual-band absorption characteristics of the proposed design.

2. DESIGN AND SIMULATION OF STRUCTURE

Figure 1 shows the schematic of the proposed terahertz metamaterial absorber, which consists of two metallic elements: top metal layer and lower metallic ground plane, separated by an isolation material spacer. The top metallic layer includes two distinct resonant structures, a

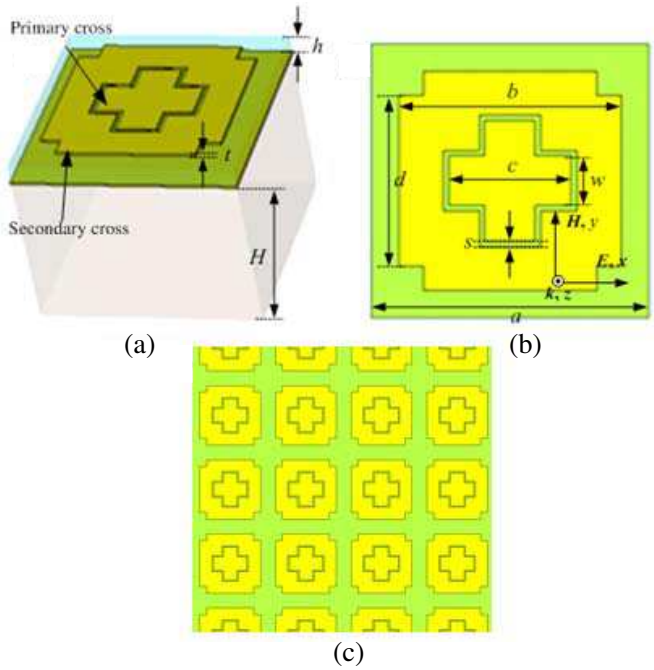

Figure 1. Structure schematic of dual-band terahertz metamaterial absorber: (a) perspective view, (b) top view and (c) the periodical arrays.

primary metallic cross resonator and a surrounding secondary metallic cross resonator with the former in the center of the latter, as shown in Fig. 1(a). The two cross resonators can be thought as a new type of electric ring resonators (ERRs) [28, 29], and couple strongly to uniform electric fields and weakly to the magnetic fields, providing two different frequency dependent electric responses $\varepsilon_1(\omega)$ and $\varepsilon_2(\omega)$. However, by combining two resonators with a metallic ground plane, the magnetic component of EM wave couples between two resonators and the ground plane, thus generating two different antiparallel currents resulting in two different frequency dependent magnetic responses $\mu_1(\omega)$ and $\mu_2(\omega)$ [30]. By adjusting the amplitude and frequency location of the electric response and corresponding magnetic response, the impedance of the absorber can match to the wave impedance of free space approximately, realizing the minimal reflectance at a specific frequency. In addition, the metallic ground plane is thicker than the penetration depth of terahertz wave and the transmission of absorber is zero. Therefore, these two conditions can realize the high performance and dual-band terahertz absorber using such metamaterial.

To verify designed rationality and understand the physical mechanisms of our proposed dual-band metamaterial absorber, the structure was constructed on silicon substrate with complex dielectric constants of $\varepsilon = 11.9 + 0.0476i$, while the polyimide of $\varepsilon = 2.88 + 0.144i$ was used as the isolation material spacer layer between two metallic layers, and two metallic layers were modeled as lossy gold film with an electric conductivity 4.09×10^7 S/cm. The optimized dimensions of the proposed absorber structure are shown in Table 1. The electromagnetic properties of the absorber were calculated using the FDTD method, where the periodic boundary conditions were set properly and the wave vector was perpendicular to the absorber plane, as shown in Fig. 1(b), while Fig. 1(c) shows the period arrays of unit cell.

Figure 2 shows the calculated distributions of the electric field and surface current at resonances for the ERRs and ground plane. In Figs. 2(a), (b), (c) and (d), we can clearly see that the tangential component (x-component) of the electric fields in the surface of the ERRs is much stronger than the normal component (z-component). The electric field concentrates strongly in gap between two ERRs as

Table 1. Dimensions of terahertz metamaterial absorber (all units in μm).

Parameters	H	h	t	a	b	d	c	w	s
Values	500	4	0.5	50	40	31	22	9	3

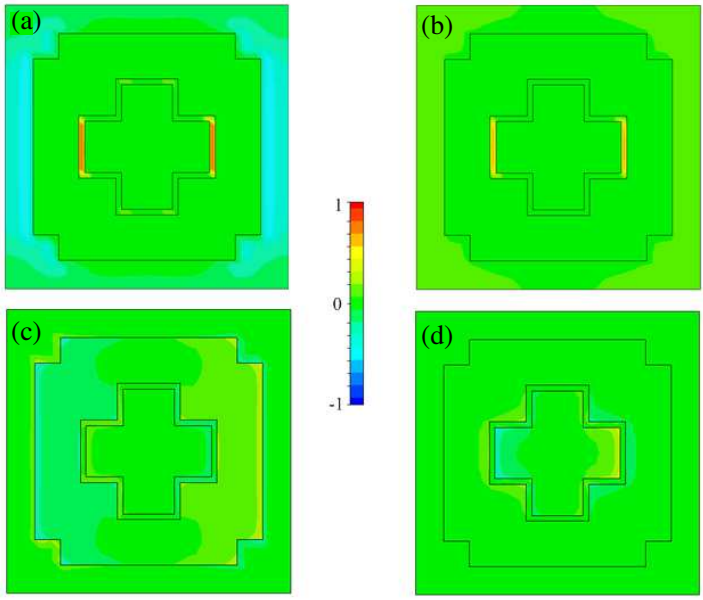

Figure 2. Calculated electric field distribution for the ERRs and ground plane: (a) and (b) show the x-component of the electric field of the ERRs at low and high frequencies, respectively; (c) and (d) show the z-component of the electric field of the ERRs at low and high frequencies, respectively.

well as at the edges of secondary ERR at low resonant frequency (Fig. 2(a)), and in gap between two ERRs at high resonant frequency (Fig. 2(b)), indicating a strong coupling between the incident wave and the electric resonance in the ERRs. While the calculated surface current on top two resonant structures and lower ground plane for low and high resonance frequencies are displayed in Figs. 3(a), (b), (c) and (d), respectively. It is evident that there are the magnetic response associated with the antiparallel conductive current in the resonator and the ground plane as well as the displacement current in dielectric between the resonator and the ground plane. Therefore, these results verify that the absorber is correctly coupling to the incident electric and magnetic field, as we expected.

By tuning the electric and magnetic resonances individually, we are able to create a condition such that the absorber is impedance-matched to the free space value in a special region. Thus, the absorber can strongly couple and absorb the EM wave when they share a center resonant frequency simultaneously [31]. Fig. 4 shows

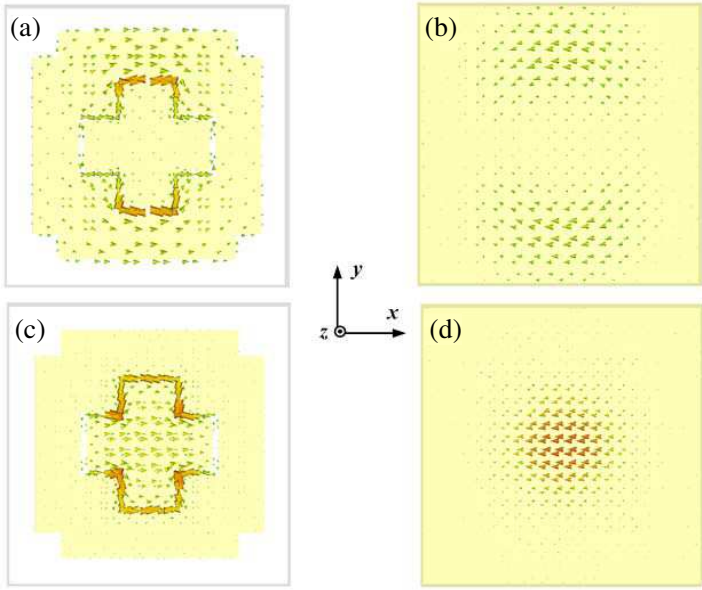

Figure 3. Calculated surface current distribution for the ERRs and ground plane: (a) and (b) show the anti-parallel currents of the secondary cross resonator and ground plane induced by magnetic coupling at low resonant frequency, respectively; (c) and (d) show the anti-parallel currents of the primary cross resonator and ground plane induced by magnetic coupling at low resonant frequency, respectively.

the calculated magnitude of the reflection S_{11} and absorption A, relative impedance z, and phase of the reflection S_{11} as a function of frequency under normal incidence. It can be observed from Fig. 4(a) that the reflection magnitude of the absorber is high at low frequency region, then undergoes two minimum values near 1.71 and 3.56 THz respectively, and finally goes up again, while the transmission magnitude is zero because the metallic ground plane is thicker than the penetration depth of terahertz wave (not shown in Fig. 4(a)). Thus, the reflectance spectrum results in two absorption peaks at the corresponding frequency (near 1.71 and 3.56 THz). Moreover, each with absorptions by $A = 1 - (S_{11})^2$ overs 99.94%, and the full widths at half maximum (FWHM) are 0.14 and 0.24 THz for the low and high frequency peaks respectively, while the off-resonance absorption is very low. As can be seen from above calculated results, the perfect absorption with very narrow band only occurs near resonant frequency. Such as, the absorption is less than 20% around the frequency ranges

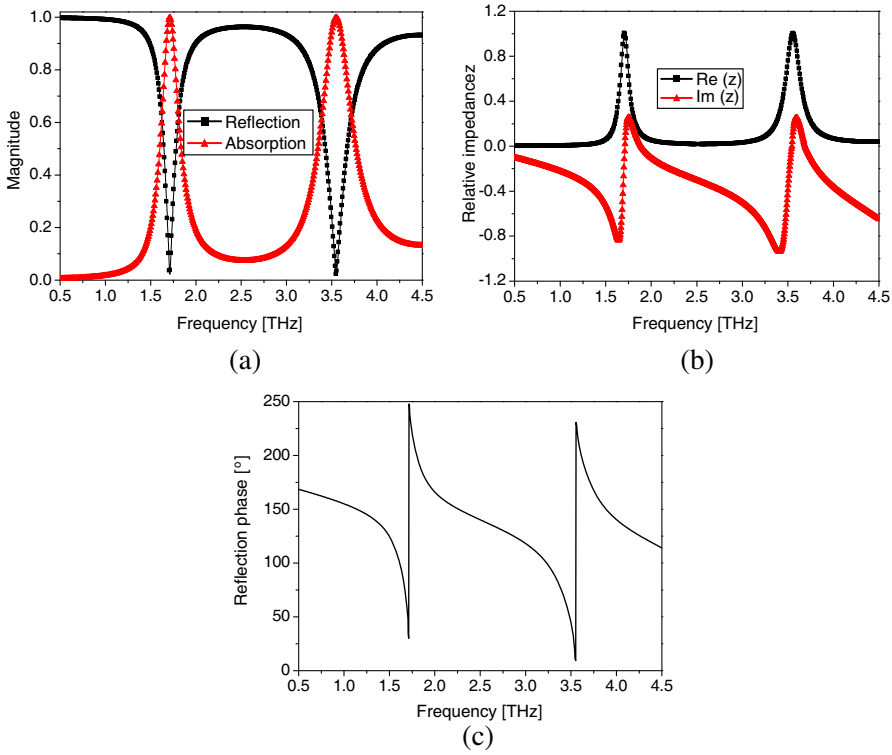

Figure 4. Calculated results for the proposed terahertz metamaterial absorb under normal incidence: (a) magnitude of reflection and absorption, (b) relative impedance of retrieved extracted from calculated results, and (c) reflection phase.

from 0.5 to 1.5 THz, 2 to 3.14 THz and 4.06 to 4.5 THz. Therefore, such narrow band response absorber has significant potential applications, including the bolometric pixel elements due to its nearly perfect conversion from EM energy to heat, and the spectrum filters due to the resonant narrow band response [30].

To better understand the mechanism of the above high absorption, the relative impedance z was extracted from the calculated scattering parameter, and the expression is as follow [32]:

$$z(\omega) = \left[(1 + S_{11})^2 / (1 - S_{11})^2 \right]^{1/2}$$

According to above extracted expression, Fig. 4(b) shows the extracted real and imaginary part of relative wave impedance z under normal incidence. At the absorptive peaks of 1.71 and 3.56 THz, the

absorber achieves near perfect impedance matched to the free space, where the real part of relative impedance z is near unity, $\mathrm{Re}(z) \approx 1$, and the imaginary part is minimized, $\mathrm{Im}(z) \approx 0$, thus resulting in near zero reflection, indicating that the imaginary part of the refraction index n is quite large providing a large wave attenuation [20]. Here, the effective refractive index of the metamaterial absorber cannot be accurately obtained by the retrieval algorithm because the transmission S_{21} is zero for all the frequency bands. But we roughly evaluate it from the relation of the refractive index with scattering parameters, i.e., $e^{ink_0d} = S_{21}/[1 - S_{11}(z-1)/(z+1)]$. In order to make the right side of the equation to be zero, the imaginary part of the refractive index should be very large [33]. While Fig. 4(c) exhibits the reflection phase of the absorber under normal incidence, the reflection phase firstly decreases with the increasing of the frequency, reaches a minimum value at low resonant frequency (1.71 THz) and jumps to a maximum value abruptly. With the frequency increasing continuously, the reflection phase decreases sequentially and again reaches another minimum value at high resonant frequency (3.56 THz), then suddenly changes from minimum to maximum, and finally continues to decrease with the increasing of the frequency. This phenomenon could be explained as the fact that at resonance frequency opposite charges are accumulated between two cross resonators, forming a capacitance, further enhancing the strength of resonance and absorption. This is similar to the diode in off state existing between ERRs, as shown in previous tunable electromagnetic metamaterial reflector/absorber [34]. Thus, two sudden phase jumps further indicate the dual band resonant frequencies and strong absorption of the absorber.

To further understand physical mechanism of dual-band absorption, the power flow in the terahertz absorber was calculated to analyze how and where the absorption happens [24]. Fig. 5 shows the power flow of the terahertz absorber at two peak frequencies. Fig. 5(a) shows the power flow from a view along the y-direction (in the xz-plane) for low frequency, while Fig. 5(b) shows high frequency. For low frequency, we note that the input power flow at input port are parallel streams each other. As gradually shifting to the absorber, most of streams will flow across the secondary resonant structure, curl in the isolation material and finally are congregated in isolation material, as shown in Fig. 5(a). However, for high frequency, the streams are different from the low frequency. They flow directly into the isolation material by the space between the primary and secondary structures, subsequently concentrate in isolation material, as shown in Fig. 5(b). At the same time, the three dimensional distributions of the power flow for low and high frequency are also plotted in Figs. 5(c) and (d) respectively, which

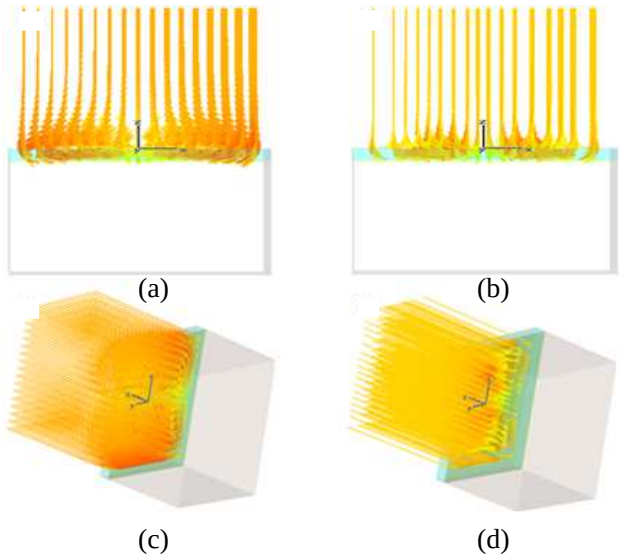

Figure 5. Distributions of the power flow in the absorber: (a) and (b) are xz-plane, and (c) and (d) are 3D distribution of the power flow, at low and high resonant frequencies respectively.

illustrate the detail distributions of power flow. These results indicate that the absorber is a promising EM wave collector, which traps the input power into specific positions of the devices and then strongly absorbs it.

As previous discussions, we note that the absorption arises from not the ohmic loss of the metal but the dielectric loss of the isolation material [35]. Fig. 6 shows the calculated absorption results of different loss tangent $\tan(\delta)$ of dielectric. Fig. 6(a) shows that the calculated results start from a lossless isolation material ($\tan(\delta) = 0$) and gradually increase $\tan(\delta)$ to 0.14, while Fig. 6(b) shows that the influence of loss tangent on tow absorption peaks. The absorber shows different absorption responses at two resonant frequencies with increasing $\tan(\delta)$, which has two different behaviors: a rapid enhancement and a gradual decrease. First, it can be seen that at two peak frequencies (1.71 THz and 3.56 THz), only 75.1% and 77.3% energy are absorbed respectively when the isolation material is lossfree ($\tan(\delta) = 0$). This indicates that the absorption mainly comes from the Ohmic losses of the ERRs. Then, two absorption peaks are rapidly enhanced to the maximum values 99.98% simultaneously when the $\tan(\delta)$ increases from zero to 0.05. These show that only

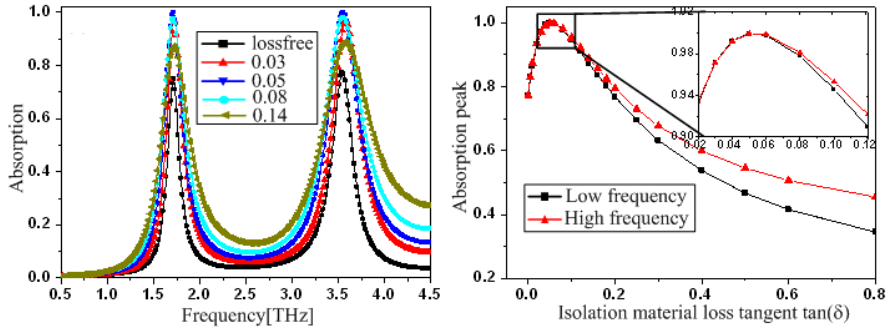

Figure 6. (a) Absorption and (b) two peak absorptions spectra with increasing loss tangent $\tan(\delta)$.

below 25% energy is collected and consumed in dielectric, which come from the high density resonant current losses. Finally, two absorption peaks gradually drop back and are even lower than that of lossfree when the $\tan(\delta)$ is further increased, which is in accord with previous results [25]. Therefore, these results reveal that the major component responsible for absorption in our absorber structure is Ohmic losses, and calculation indicates that this is three times larger than the dielectric loss. This is consistent with studies of near-perfect absorption at visible frequency where it was found that dielectric absorption was relatively insignificant in comparison to metallic absorption [36].

3. POLARIZATION INSENSITIVE AND WIDE ANGLE ABSORPTION

To examine the sensitivity to polarization, we analyzed the absorptive characteristics under normal incident plane wave with different electric field polarizations. In order to conveniently describe, the polarization angle ϕ is defined as the angle between electric field ($\mathbf{E}$) and x-axis. The calculated results for different polarizations are shown in Fig. 7. We could clearly see that the absorption can maintain maximum values 99.93% around 1.71 and 3.56 THz for different polarizations with normal incident wave. Thus, we could assure that 1.71 and 3.56 THz are the center resonant frequency points of dual-band absorber. Moreover, as the ϕ increasing, two absorptive peak magnitudes and resonance frequencies are nearly unchanged due to the high degree symmetry of the resonant structure. Therefore, these results demonstrate that the proposed terahertz metamaterial absorber

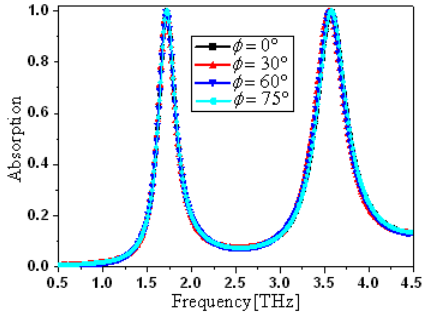

Figure 7. Absorption curves for different polarization angle ϕ at normal incidence.

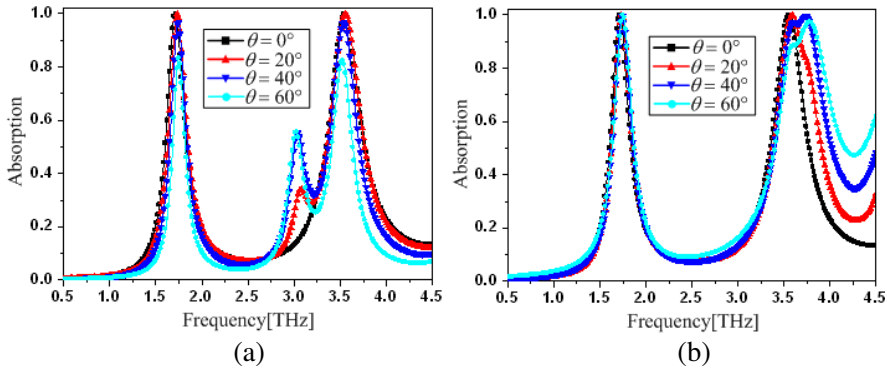

Figure 8. Absorption curves for different oblique incidences at $\phi = 0$: (a) TE modes and (b) TM modes.

is insensitive to the polarization of incident EM wave.

For above discussions, we obtained the absorption under normal incidence. However, in practical applications, EM wave are usually incident onto absorbers with an oblique incident angle, so it is necessary to investigate the absorption under oblique incidence. Fig. 8 shows the calculated absorption curves under incident angle $\theta = 0°$, $20°$, $40°$ and $60°$ respectively (at $\phi = 0$). It is observed from Fig. 8(a) that for TE waves, the two absorptive peaks remain greater than 97% for the incident angle ranging from $0°$ to $40°$. With the incident angle increasing, the absorption peak monotonously decreases, but the low frequency and high frequency still have 83.2% and 82.4% absorptions for the incident angle of $60°$, respectively. This could be explained as the fact that with the increase of incident angle,

the incident magnetic flux between the metallic layers comes to be less and less. It is therefore less effective to drive a strong magnetic resonance. Thus, only the electric resonance is dominant, and most of the EM energy of the incident wave is reflected back caused by the intense impedance mismatch [32]. For the TM wave case, the two absorptions are almost unchanged for all of the incident angles with peak absorption above 97.3%, as shown in Fig. 8(b), but the center frequency of the high frequency absorption peak has a shift about 0.22 THz as the incident angle increasing from 0° to 60°. Surprisingly, for off-normal incident an additional spectral peak emerges for the absorber at around 3.0 THz but only in the TE polarization mode. The similar feature also occurs in previous isotropic metamaterial [37], which was already predicted theoretically by numerically studying the frequency response of negative magnetic artificial media. It was thus shown that this phenomenon is due to a zero in the permeability dispersion $\mu(\omega)$ around magnetic plasmas frequency. Moreover, the theoretical analysis further demonstrated this extra feature results from the intrinsic dispersion of the effective parameters rather than structuring [38]. Therefore, from the above calculated results, it is clear that the designed terahertz metamaterial absorber can works well over a large range of incident angle for both TE and TM wave modes.

4. FABRICATION AND MEASUREMENT

To verify the correctness of calculated results, we fabricated the absorber with a surface micromachining process on a silicon wafer with 500 μm thickness. A 2 μm-thick SiO_2 layer was deposited on the Si substrate using plasma enhanced chemical vapor deposition (PECVD). A 200 nm-thick Au/Ti film was E-beam evaporated to form the ground plane. A 4 μm-thick polyimide layer was spin coated on the top of the ground plane to form the dielectric spacer. Another 200 nm-thick Au/Ti was patterned using standard negative lithography, metal E-beam evaporation, and metal liftoff. The fabricated absorber was measured by a microscope and a THz-TDS system with an incident direction of 30 degrees from the normal direction, which is similar the previous measurement method [18], respectively.

Figure 9(a) shows the microscopic images of a unit cell and a portion of the fabricated absorber, while Fig. 9(b) shows the measured absorption curve as a function of the frequency at 30 angles of incidence. The fabricated absorber has two strong absorption peaks: an absorption peak of 82.8% around 1.724 THz and another absorption peak of 86.8% around 3.557 THz, confirming that the dual-band absorption is realized in our as-fabricated absorber. But, the fabricated

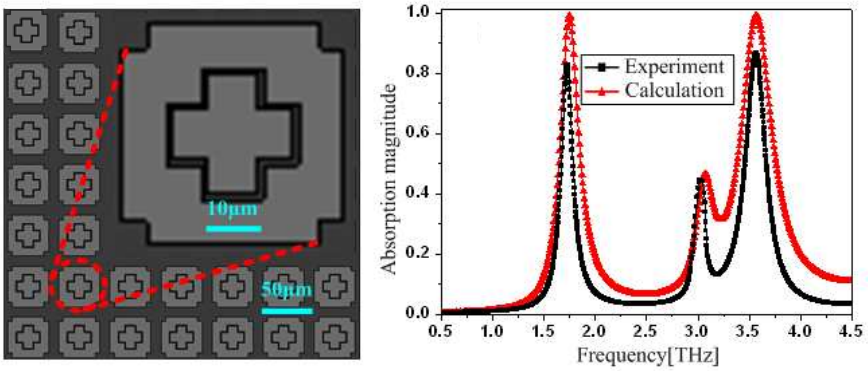

(a) (b)

Figure 9. Dual-band terahertz metamaterial absorber: (a) Microscopic images of a unit cell and a portion of the fabricated absorber, and (b) absorption curves of calculation and measurement at 30 angles of incidence.

sample exhibits not only lower absorption but also a red-shift in both absorptive peaks comparing to the calculatedly optimized results. For example, the first absorption peak has reduced by 16.4% and shifted by 20 GHz respectively, while the second absorption peak has reduced by 12.4% and shifted by 11 GHz respectively. These differences are reasonably ascribed to some deviations from the designed structure in the shape and size due to fabrication tolerances. For example, the split gap is somehow narrower, and the corners of the ERRs are slightly rounded (as shown in Fig. 9(a)). Especially, it should be noted that values used in calculation for the polyimide spacing layer were estimated based on published values at lower GHz frequencies. Further, the thickness of the polyimide layer was measured to be closer to 4.4 μm rather than the 4 μm used in calculations, since this distance determines the frequency location of the magnetic resonances.

5. CONCLUSION

In summary, a polarization-insensitive and wide-angle terahertz metamaterial absorber with dual bands has been successfully designed, fabricated and measured. To better understand the physical mechanism of the dual-band terahertz metamaterial absorber, electric field and surface current distributions, relative impedance, power flow distributions, and dielectric absorption were plotted, which demonstrated that the absorber is not only correctly coupling to the

incident electric and magnetic field, but also can trap the input power into specific positions of the devices and absorb it. To analyze the polarization and wide-angle performances of the proposed absorber, absorption characteristics were investigated for differently polarized and incident directions of incident TE or TM wave, which shows that the absorber is insensitive to polarization and incident angle of the TE or TM wave. Moreover, the experiment further demonstrated that the fabricated absorber has two strong absorption peaks: an absorption peak of 82.8% around 1.724 THz, and another absorption peak of 86.8% around 3.557 THz. Therefore, this structure feature can provide more flexible design in multi-band absorptions by combining resonant structures and can be readily extended to infrared and visible frequencies.

ACKNOWLEDGMENT

The work is supported by the National Natural Science Foundation of China (51005001), the China Postdoctoral Science Foundation (20090450226), the Research Foundation of Education Bureau of Heilongjiang Province (11551098 and 11531055) and Youth Foundation of Harbin University of Science and Technology (2009YF024 and 2009YF025).

REFERENCES

1. Veselago, V. G., "The electrodynamics of substances with simultaneously negative values of ε and μ," *Sov. Phys. Usp.*, Vol. 10, 509–514, 1968.
2. Smith, D. R., W. J. Padilla, D. C. Vier, S. C. Nemat-Nasser, and S. Schultz, "Composite medium with simultaneously negative permeability and permittivity," *Phys. Rev. Lett.*, Vol. 84, 4184–4187, 2000.
3. Zhou, H., Z. Pei, S. Qu, S. Zhang, J. Wang, Q. Li, and Z. Xu, "A planar zero-index metamaterial for directive emission," *Journal of Electromagnetic Waves and Applications*, Vol. 23, No. 7, 953–962, 2009.
4. Feise, M. W., P. J. Bevelacqua, and J. B. Schneider, "Effects of surface waves on behavior of perfect lenses," *Phys. Rev. B*, Vol. 66, 035113, 2002.
5. Pendry, J. B., "Negative refraction makes a perfect lens," *Phys. Rev. Lett.*, Vol. 85, 3966–3969, 2000.

6. Alici, K. B. and E. Ozbay, "Electrically small split ring resonator antennas," *J. Appl. Phys.*, Vol. 101, 083104, 2007.
7. Hwang, R. B., H. W. Liu, and C. Y. Chin, "A metamaterial-based E-plane horn antenna," *Progress In Electromagnetics Research*, Vol. 93, 275–289, 2009.
8. Tang, Y., B. A. Jeremy, D. H. Werner, and T. S. Mayer, "Single-layer metallodielectric nanostructures as dual-band midinfrared filters," *Appl. Phys. Lett.*, Vol. 92, 263106–263108, 2008.
9. Bonache, J., I. Gil, J. Garcia-Garcia, and F. Martin, "Novel microstrip bandpass filters based on complementary split-ring resonators," *IEEE Trans. Microw. Theory Tech.*, Vol. 54, 265, 2006.
10. Sabah, C. and S. Uckun, "Multilayer system of lorentz/drude type metamaterials with dielectric slabs and its application to electromagnetic filters," *Progress In Electromagnetics Research*, Vol. 91, 349–364, 2009.
11. Siso, G., M. Gil, J. Bonache, and F. Martin, "Application of metamaterial transmission lines to design of quadrature phase shifters," *Electron. Lett.*, Vol.43, No. 20, 1098–1100, 2007.
12. Khalilpour, J. and M. Hakkak, "S-shaped ring resonator as anisotropic uniaxial metamaterial used in waveguide tunneling," *Journal of Electromagnetic Waves and Applications*, Vol. 23, No. 13, 1763–1772, 2009.
13. Wakatsuchi, H., S. Greedy, C. Christopoulos, and J. Paul, "Customised broadband metamaterial absorbers for arbitrary polarization," *Opt. Express*, Vol. 18, 22187–22198, 2010.
14. Wang, B.-N., T. Koschny, and C. M. Soukoulis, "Wide-angle and polarization-independent chiral metamaterial absorber," *Phys. Rev. B*, Vol. 80, 33108–33111, 2009.
15. Zhu, B., Z. Wang, C. Huang, Y. Feng, J. Zhao, and T. Jiang, "Polarization insensitive metamaterial absorber with wide incident angle," *Progress In Electromagnetics Research*, Vol. 101, 231–239, 2010.
16. Wang, J., S. Qu, Z. Fu, H. Ma, Y. Yang, X. Wu, Z. Xu, and M. Hao, "Three-dimensional metamaterial microwave absorbers composed of coplanar magnetic and electric resonators," *Progress In Electromagnetics Research Letters*, Vol. 7, 15–24, 2009.
17. Zhu, B., C. Huang, Y. Feng, J. Zhao, and T. Jiang, "Dual band switchable metamaterial electromagnetic absorber," *Progress In Electromagnetics Research B*, Vol. 24, 121–129, 2010.
18. Tao, H., N. I. Landy, C. M. Bingham, X. Zhang, R. D. Averitt,

and W. J. Padilla, "A metamaterial absorber for the terahertz regime: Design, fabrication and characterization," *Opt. Express*, Vol. 16, 7181–7188, 2008.

19. Tao, H., C. M. Bingham, A. C. Strikwerda, D. Pilon, D. Shrekenhamer, N. I. Landy, K. Fan, X. Zhang, W. J. Padilla, and R. D. Averitt, "Highly flexible wide angle of incidence terahertz metamaterial absorber: Design, fabrication, and characterization," *Phys. Rev. B*, Vol. 78, 241103(R), 2008.
20. Landy, N. I., C. M. Bingham, T. Tyler, N. Jokerst, D. R. Smith, and W. J. Padilla, "Design, theory, and measurement of a polarization-insensitive absorber for terahertz imaging," *Phys. Rev. B*, Vol. 79, 125104–125109, 2009.
21. Gu, C., S. Qu, Z. Pei, H. Zhou, J. Wang, B.-Q. Lin, Z. Xu, P. Bai, and W.-D. Peng, "A wide-band polarization-insensitive and wide-angle terahertz metamaterial absorber," *Progress In Electromagnetics Research Letters*, Vol. 17, 171–179, 2010.
22. Zhou, Q. L., C. L. Zhang, K. J. Mu, B. Jin, L. L. Zhang, W. W. Li, and R. S. Feng, "Optical property and spectroscopy studies on the explosive 2,4,6-trinitro-1,3,5-trihydroxybenzene in the terahertz range," *Appl. Phys. Lett.*, Vol. 92, 101106–101108, 2008.
23. Zhang, L. L., H. Zhong, C. Deng, C. L. Zhang, and Y. J. Zhao, "Terahertz wave reference-free phase imaging for identification of explosives," *Appl. Phys. Lett.*, Vol. 92, 091117–091119, 2008.
24. Wen, Q. Y., H. W. Zhang, Y. S. Xie, Q. H. Yang, and Y. L. Liu, "Dual band teraherz metamaterial absorber: Design, fabrication, and characterization," *Appl. Phys. Lett.*, Vol. 95, 241111-3, 2009.
25. Tao, H., C. M. Bingham, D. Pilon, K. Fan, A. C. Strikwerda, D. Shrekenhamer, W. J. Padilla, X. Zhang, and R. D. Averitt, "A dual band terahertz metamaterial absorber," *J. Phys. D: Appl. Phys.*, Vol. 43, 225102-6, 2010.
26. Tonouchi, M., "Cutting-edge terahertz technology," *Nature Photonics,* Vol. 1, 97–105, 2007.
27. Liu, X. L., T. Starr, A. F. Starr, and W. J. Padilla, "Infrared spatial and frequency selective metamaterial with near-unity absorber," *Phys. Rev. Lett.*, Vol. 104, 207403, 2010.
28. Padilla, W. J., M. T. Aronsson, C. Highstrete, M. Lee, A. J. Taylor, and R. D. Averitt, "Electrically resonant terahertz metamaterials: Theoretical and experimental investigations," *Phys. Rev. B*, Vol. 75, 041102(R), 2007.
29. Schurig, D., J. J. Mock, B. J. Justice, S. A. Cummer, J. B. Pendry, A. F. Starr, and D. R. Smith, "Metamaterial electromagnetic

cloak at microwave frequencies," *Science*, Vol. 314, No. 5801, 977–980, 2006.

30. Landy, N. I., S. Sajuyigbe, J. J. Mock, D. R. Smith, and W. J. Padilla, "Perfect metamaterial absorber," *Phys. Rev. Lett.*, Vol. 100, 207402, 2008.
31. Smith, D. R., J. Gollub, J. J. Mock, W. J. Padilla, and D. Schurig, "Calculation and measurement of bianisotropy in a split ring resonator," *J. Appl. Phys.*, Vol. 100, 024507, 2006.
32. Li, M. H., H. L. Yang, and X. W. Hou, "Perfect metamaterial absorber with dual bands," *Progress In Electromagnetics Research*, Vol. 108, 37–49, 2010.
33. Huang, L. and H. Chen, "Multi-band and polarization insensitive metamaterial absorber," *Progress In Electromagnetics Research*, Vol. 113, 103–110, 2011.
34. Zhu, B., Y. J. Feng, J. M Zhao, C. Huang, Z. B. Wang, and T. Jiang, "Polarization modulation by tunable electromagnetic metamaterial reflector/absorber," *Optics Express*, Vol. 18, 23196–23203, 2010.
35. Hu, C. G., X. Li, Q. Feng, X. N. Chen, and X. G. Luo, "Investigation on the role the dielectric loss in metamaterial absorber," *Optics Express*, Vol. 18, 6598–6603, 2010.
36. Hu, C., Z. Zhao, X. Chen, and X. Luo, "Realizing near-perfect absorption at visible frequencies," *Optics Express*, Vol. 17, 11039–11044, 2009.
37. Koschny, T., L. Zhang, and C. M. Soukoulis, "Isotropic three-dimensional left-handed metamaterials," *Physical Review B*, Vol. 71, 121103(R), 2005.
38. Zhang, F. L., Q. Zhao, L. Kang, J. Zhou, and D. Lippens, "Experimental verification of isotropic and polarization properties of high permittivity-based metamaterial," *Physical Review B*, Vol. 80, 195119, 2009.